Elucidation of the molecular structure of hydrated vanadium oxide species by X-ray absorption spectroscopy: correlation between the V···V coordination number and distance and the point of zero charge of the support oxide†

Daphne E. Keller, Diek C. Koningsberger and Bert M. Weckhuysen*

Received 11th July 2006, Accepted 4th September 2006
First published as an Advance Article on the web 19th September 2006
DOI: 10.1039/b609757j

The effect of the point of zero charge (PZC) of the support oxide (Al_2O_3, Nb_2O_5, SiO_2 and ZrO_2) on the molecular structure of hydrated vanadium oxide species has been investigated with EXAFS spectroscopy for low-loaded vanadium oxide catalysts. It was found that the degree of clustering (*i.e.*, the V···V coordination number) and the V···V distance increase with decreasing PZC of the support oxide; *i.e.*, Al_2O_3 (8.7) < ZrO_2 (7) < Nb_2O_5 (3.3) < SiO_2 (2). Upon hydration the silica-supported vanadium oxide exhibited a clear alteration in the position of the oxygen atoms surrounding the central vanadium atom and the number of oxygen atoms around vanadium increased to five. In contrast, only minor changes in the molecular structure were detected for the alumina-, niobia- and zirconia-supported vanadium oxide catalysts. Based on a detailed analysis of the EXAFS data a semi-quantitative distribution of vanadium oxide species present on the surface of the different support oxides can be obtained, which is in good agreement with earlier characterization studies primarily making use of Raman spectroscopy.

Introduction

The dynamic nature of supported vanadium oxide species has been shown to lead to structural changes upon hydration of supported vanadium oxide catalysts.[1,2] The extent of hydration, the vanadium oxide loading and the type of support oxide are known to influence the molecular structure of vanadium oxide species under ambient and hydrated conditions.[3–7] Hydrated vanadium oxide species can be of interest for the understanding of their catalytic action. H_2O is formed during some reactions which may lead to the (partial) hydration of the catalyst surface.[7] Also the hydration mechanism may give insight into the preparation of the catalyst materials, as well as into the influence of catalyst storage under ambient conditions.

Hazenkamp and Blasse [8] suggested for silica-supported catalyst vanadium oxide that decavanadate is present when the catalyst material is in its hydrated form. Yoshida *et al.* indicated that the coordination of vanadium in hydrated silica-supported vanadium oxide catalysts is octahedral on the basis of XANES analysis.[9] Hydration phenomena have been studied for other support oxides as well. For example, in the case of MCM-41-supported vanadium oxide catalysts a pseudo-octahedral environment has been found with UV-Vis and NMR spectroscopies. Furthermore, Solsona *et al.* suggested that the (pseudo-) octahedral coordination was reached through the adsorption of one or two H_2O molecules on the supported vanadium oxide cluster.[10] Water coordination was suggested earlier by Anpo *et al.* and Morey *et al.* to explain the dramatic colour change in silica-supported vanadium oxide samples upon hydration.[11,12] On the basis of NMR data of titania-supported vanadium oxides, Gro Nielsen *et al.* concluded that vanadium was six-coordinated with one short (V═O) and one long (V–O) axial bond.[13] Silversmit *et al.* used EXAFS to determine the structure of a low-loaded vanadium-on-titania catalyst. They found an V_2O_5 resembling octahedral coordination with one short V═O bond of 1.6 Å, 4 longer V–O bonds of 2 Å and one long V–O bond of 2.2 Å.[14] Ruitenbeek *et al.* came to the conclusion on the basis of EXAFS that for a hydrated high-loaded alumina-supported catalyst the vanadium was 4 coordinated with one V═O bond of 1.55 Å, one V–OH bond of 1.74 Å and two V–O bonds of 1.90 Å.[15–17] A similar structure has been suggested by Went *et al.* when studying low-loaded silica-, alumina- and titania-supported vanadium oxide catalysts.[3]

Apparently, variations in the vanadium oxide loading, support oxide and measurement conditions complicate the determination of the molecular structure of hydrated supported vanadium oxide catalysts making use of X-ray absorption spectroscopy. Although clustering of vanadium oxide species upon hydration of the sample has often been suggested,[4,8,18,19] only a limited number of research groups have investigated the presence of vanadium atoms in the second coordination shell.[14,20] Silversmit *et al.* detect additional cations in their hydrated sample (CN = 2, R = 3.5 Å), however, they were not able to distinguish between the support cation (Ti) and a neighbouring vanadium atom.[14]

Inorganic Chemistry and Catalysis, Department of Chemistry, Utrecht University, P.O. Box 80083, 3508 TB Utrecht, The Netherlands. E-mail: b.m.weckhuysen@chem.uu.nl

† The HTML version of this article has been enhanced with colour images.

Inumaru *et al*. concluded on the basis of the FT of their EXAFS data that the V···V contribution in their spectrum increased with the support material: $MgO < Al_2O_3 < SiO_2$.[20]

In general, the molecular structure of vanadium oxide species in an aqueous environment, for example on a fully hydrated supported vanadium oxide catalyst, is dictated by the concentration of the vanadium oxide species and the pH of the water layer on top of the support surface, which in turn is determined by the point of zero charge (PZC) of the support oxide.[4] The relation between the vanadium oxide concentration, the pH of the solution and the resulting molecular structure of the vanadium oxide species is illustrated in the so-called predominance diagram.[21] Based on this diagram and the PZC of the silica surface Wachs and co-workers proposed that upon hydration silica-supported vanadium catalysts consist of a mixture of V_2O_5, $V_{10}O_{26}(OH)_2$ and $VO(OH)_3$, whereas for alumina-supported vanadium oxide catalysts $VO_3(OH)$ and V_2O_7 were predicted to be present.[4,5,22,23] The hydrated structure is also influenced by the vanadium oxide loading, and thus the vanadium oxide species are in a more polymerized state at high vanadium oxide concentrations. Vanadium oxide species are acidic and thus lower the pH of the solution above the support surface, implying that the effect of the support on the molecular structure will be most pronounced at low vanadium oxide loadings.

In this paper the effect of the support oxide material on the molecular structure of the hydrated vanadium oxide species has been investigated for a series of low-loaded vanadium oxide catalysts making use of X-ray absorption spectroscopy. A series of 1 wt% vanadium oxide catalysts were prepared on Al_2O_3, Nb_2O_5, SiO_2 and ZrO_2 as support oxides. These catalysts were allowed to fully hydrate by storing them in a moisture-rich environment. EXAFS measurements on the supported vanadium oxide catalysts enabled us to determine the local structure of the hydrated vanadium oxide species. Moreover, the vanadium oxide–support interface could be determined by combining the EXAFS data with structural modelling. The hydrated structure differed from the molecular structure after dehydration, although the extent of the differences in molecular structure clearly depends on the support oxide. The number of vanadium atoms in the second coordination shell, and thus the degree of vanadium oxide clustering, increased with decreasing PZC of the support oxide; *i.e*., Al_2O_3 (8.7) > ZrO_2 (7) > Nb_2O_5 (3.3) > SiO_2 (2). The same trend was observed for the V···V distance of the vanadium oxide species present at the support surface. Based on a detailed analysis of the EXAFS spectra a semi-quantitative distribution of surface vanadium oxide species is proposed, which will be compared with literature data mainly based on the use of Raman spectroscopy. It will be shown that X-ray absorption spectroscopy is able to corroborate the predictions made earlier by Raman spectroscopy. Furthermore, it allows the gathering of structural information on the mode of interaction between the support oxide and surface vanadium oxide species in the hydrated state.

Experimental

1. Catalyst preparation

A series of supported vanadium oxide catalysts with 1 wt% vanadium oxide loading was prepared using γ-Al_2O_3 (home made, S_{BET} = 165 $m^2\ g^{-1}$, V_{pore} = 0.35 ml g^{-1}), SiO_2 (home made, pore volume of 0.70 ml g^{-1} and surface area of 600 $m^2\ g^{-1}$), Nb_2O_5 (CBMM, HY-340, pore volume of 0.18 ml g^{-1} and surface area of 188 $m^2\ g^{-1}$) and ZrO_2 (Gimex, RC 100, pore volume of 0.23 ml g^{-1} and surface area of 100 $m^2\ g^{-1}$) as support oxides. The SiO_2 and Al_2O_3 supports were prepared *via* the sol-gel method according to a slightly altered literature recipe,[24] HNO_3 was used as the acidifying agent instead of HCl to reach a pH of 6 and 6.5 respectively, at which the gel was formed. After aging the gels for one night at room temperature the gels were dried at 303 K for 72 h. Subsequently the gels underwent a two-step calcination: 3 h at 523 K and 16 h at 823 K (SiO_2) or 973 K (Al_2O_3). The catalysts were prepared with the incipient wetness impregnation technique using a NH_4VO_3 (Merck, p.a.) solution with oxalic acid ($C_2H_2O_4 \cdot 2H_2O$, Brocacef, 99.25% pure) in a ratio of 1 : 2. The catalysts were dried at room temperature for 1 night, 1 night at 393 K and after this treatment they were calcined at 773 K for 3 h. All catalysts under investigation are listed in Table 1, together with some physicochemical data and the catalyst sample code that will be used throughout the paper.

2. EXAFS spectroscopy

XAFS experiments were carried out at beamline E4 in Hasylab (Hamburg, Germany) using a Si (111) monochromator. The measurements were performed in fluorescence mode, using an ion chamber filled with 400 mbar N_2 to determine I_0. The detector was a 7-element solid state (SiLi) detector. The

Table 1 Catalyst sample codes and some physicochemical data for all supported vanadium oxide catalysts discussed in this paper

Sample name[a]	Sample	Loading VO_x/nm^2	% Monolayer[b]		$S_{BET}/m^2\ g^{-1}$	$V_{pore}/ml\ g^{-1}$	PZC
			Monomer	Polymer			
1V–Al	1 wt% V_2O_5/Al_2O_3	0.430	18.7	5.73	165	0.35	8.7
1V–Nb	1 wt% V_2O_5/Nb_2O_5	0.399	17.3	5.32	188	0.18	3.3
1V–Si	1 wt% V_2O_5/SiO_2	0.118	5.13	1.57	594	0.71	<2.3[c]
1V–Zr	1 wt% V_2O_5/ZrO_2	0.743	32.3	9.91	100	0.23	7

[a] The sample names *x*V–M, consist of the loading in wt% (*n*), the supported metal oxide (V = vanadium) and the support cation (M = Al, Si, Nb or Zr). [b] The values for the monomeric (2.3 VO_x/nm^2) and polymeric (7.5 VO_x/nm^2) monolayer coverages are taken from Khodakov *et al*.[49] [c] Our measurements had a lower pH limit of 2.3, above which intersections between two different titration curves were not observed. Difficulties in determining a PZC value for SiO_2 have been already reported in the open literature.[41]

monochromator was detuned to 80% of the maximum intensity at the V K-edge (5465 eV) to minimize the presence of higher harmonics. The measurements were carried out in an *in situ* cell equipped with Kapton windows. Details on the cell design can be found elsewhere.[25] Data for the dehydrated (1V–$M_{support}$–D) samples were collected at 77 K after dehydration (623 K for 2 h in 2.5% O_2/He, 100 ml min^{-1}) and two or three scans were averaged. Data for the hydrated samples (1V–$M_{support}$–H) were collected at 77 K after hydration at room temperature in a closed exsiccator (desiccator) with water instead of silica-gel on the bottom below the samples. Three scans were averaged for each sample. Prior to the measurements a He–H_2O mixture (the He was led through a water containing vessel) was led over the samples for 15 min at room temperature. Raman measurements in He did not show any influence of the He on the vanadium oxide structure at room temperature.

The EXAFS data analysis was carried out using the XDAP code developed by Vaarkamp *et al.*[26] The background was subtracted employing cubic spline routines with a continuously adjustable smooth parameter.[27] This led to the normalized oscillatory part of the XAFS data, for which all the contributions to the spectrum, including the AXAFS, were maximized.[27]

The EXAFS data analysis program XDAP allows one to perform multiple-shell fitting in R-space by minimizing the residuals between both the absolute and the imaginary part of the Fourier transforms of the data and the fit. R-space fitting has important advantages compared to the usually applied fitting in k-space and is extensively discussed in a paper by Koningsberger *et al.*[27] The difference file technique was applied together with phase-corrected Fourier transforms to resolve the different contributions in the EXAFS data.[27] The details of the fit procedure has been described in previous papers by our group.[27,28]

Details of the fabrication of the phase shifts and backscattering amplitudes for V–O, V–Al, V–V, V–Si, V–Zr and V–Nb are provided in previous papers.[28,29] Values for the disorder (Debye–Waller factor: σ^2) and inner potential (E_0) are given relative to the reference data.[27]

The variances of the R-space fit give a quantitative measure of the quality of the fit.[27] Generally, values lower than 2% are acceptable. Typical values for the limits of accuracy of the EXAFS coordination parameters are: N (± 10%), R (± 5%), $\Delta\sigma^2$ (± 10%) and ΔE_0 (± 10%).[30]

3. Cerius^2 structural model

Structural models for the silica support surface were constructed using the Cerius^2 molecular modelling software.[31] A VO_4 unit was anchored to the support surface. The obtained structural model was used as an auxiliary to determine EXAFS input parameters for fitting the higher coordination shells. The final higher shells EXAFS fits were obtained after several iteration steps with the molecular model obtained from Cerius^2.

The crystalline structure for β-quartz was taken from the Cerius^2 database. The (111) surface is one of the preferentially exposed surfaces for β-SiO_2.[32] The γ-Al_2O_3 crystal was constructed from X-ray diffraction data obtained and interpreted by Zhou and Snyder.[33] The resulting crystal model was cut along the (110) plane, exposing the preferentially exposed surface.[34] The crystal of Nb_2O_5 was prepared according to the structure determined by Gruehn.[35] The oxygen terminated (001) surface has been chosen to accommodate the VO_4 cluster. The (100) surface of monoclinic ZrO_2, from the Cerius database, was found to be the most suitable to anchor the VO_4 cluster.

For the dehydrated VO_4 models on all supports, the V=O and the V–O distances were set according to the results obtained from the EXAFS analysis including V=O, V–O and V···$M_{support}$ distances. Rotation of the molecule around the $M_{support}$–O bond and bending of the V–O–$M_{support}$ bond were the only operations performed to find a suitable configuration of the molecule on top of the surface, where the V···$M_{support}$ distance was used as a structural constraint on all surfaces. An energy minimization was not performed. After rotation of the molecule to a suitable position, the distances from the vanadium atom to the nearest support cations and the nearest support oxygen atoms were determined. The final higher shells EXAFS fits for the dehydrated samples were determined after several iteration steps with the molecular model obtained from Cerius^2. For the silica-supported hydrated catalyst a structural model was also prepared. The model was constructed with the V–O and V···Si distances obtained from EXAFS as structural constraints.

Results

1. XANES spectra

The normalized XANES spectra of the 1V–Si, 1V–Nb, 1V–Zr and 1V–Al samples after hydration (solid lines) and dehydration (dashed lines) are displayed in Fig. 1. It can be seen that the influence of hydration is large for 1V–Si, but much smaller for the other catalysts. The pre-edge peak of the 1V–Si–H sample is lower in intensity and the shape of the total edge data ($5475 < E < 5510$ eV) is different. According to Wong

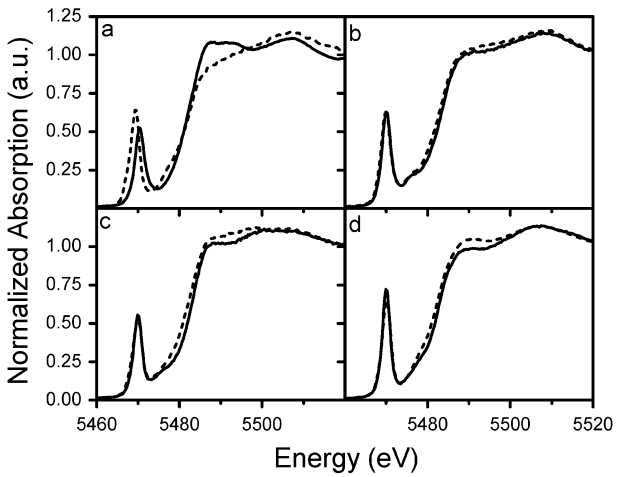

Fig. 1 The pre-edge and XANES region of the XAFS spectra of samples (a) 1V–Si, (b) 1V–Nb, (c) 1V–Zr and (d) 1V–Al, measured at 77 K after dehydration (- - -) and hydration (—).

et al.[36] the height of the pre-edge peak compared to the height of the edge-jump makes it possible to determine the local symmetry of the species found on the surface. For a perfect tetrahedron this value is 0.8–1.0. The value observed for 1V–Si–D is 0.64, indicating that the molecular structure of the vanadium oxide species resembles a distorted tetrahedron. The value observed for 1V–Si–H is 0.52, implying that the coordination geometry deviates even more from a tetrahedral symmetry. For the other samples only small differences are observed both for the height and the position in energy and of the pre-edge peak implying minor changes in the coordination symmetry.

2. EXAFS data

The EXAFS spectra of the wet (dashed lines) and dry (dotted lines) vanadium samples are shown in Fig. 2. Large differences in both amplitude and nodes are observed for 1V–Si (see Fig. 2a). The changes for the other samples are much smaller. Fig. 3 gives the corresponding FT (k^1, Δk = 2–11 Å^{-1}). For all samples the first two nodes of the imaginary parts of the FTs are remarkably similar. This part of the FT is due to a V═O coordination. A comparison of the FTs of 1V–Si–H and 1V–Si–D shows not only much lower amplitude, but also large differences for $1.5 < R < 2$ after hydration (see Fig. 3a). From all this information it can be concluded that hydration has a large influence on the coordination geometry directly around the vanadium in the 1V–Si sample. Much smaller changes in the coordination geometry are observed for the other samples. All samples show changes in the higher coordination shells ($R > 2$ Å) with the smallest changes observed in the FT for 1V–Nb.

3. EXAFS data analysis

The EXAFS data analysis of the hydrated 1V–Si–H sample was carried out in two consecutive steps. It can be seen in Fig. 3a that a node occurs in the FT of the data of 1V–Si–H around 2.3 Å. The application of a R-space fit was tried, (k^1, Δk = 2.5–11 Å^{-1}, ΔR = 0.7–2.4 Å), which allowed the use of 10.6 fit parameters.[37] A three-shell model was applied using a geometry with the following oxygen coordination: V–$O_{(1)}$ (CN = 1, R = 1.58 Å), ascribed to the V═O bond, a V–$O_{(2)}$ (CN = 3) and V···$O_{(3)}$ (CN = 1), the latter two to explain the large differences around 1.8 Å. This three-shell model requires 12 fit parameters in total. Two were kept fixed (for the V═O coordination), leading to 10 independent free parameters, which are allowed according to the Nyquist theorem.[37] The result of the three-shell fit is shown in Fig. 4. The data could be fit with one V═O coordination at 1.58 Å, three V–O bonds of 1.83 Å and one oxygen contribution at 2.37 Å (Table 2). Compared to the 1V–Si–D sample the V–O bonds are longer and an extra oxygen contribution has been introduced, most probably due to the presence of an adsorbed water molecule. It can be seen in Fig. 4 that the three-shell fit does not describe contributions of higher coordination shells ($R > 2.3$ Å).

The next step in the EXAFS data analysis was to include the higher coordination shells in order to gain information about the position of the vanadium species relative to the support

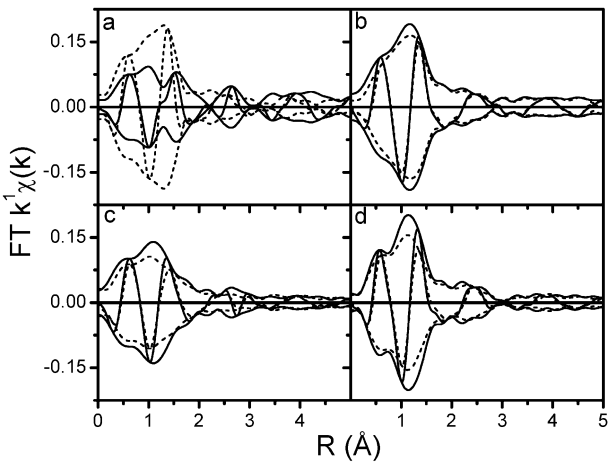

Fig. 3 The k^1 weighted FTs of the experimental $\chi(k)$ (Δk = 2.5–11 Å^{-1}, (ΔR = 0.7–5.0 Å), hydrated (—) and dehydrated (- - -) for (a) 1V–Si (b) 1V–Nb, (c) 1V–Zr and (d) V–Al.

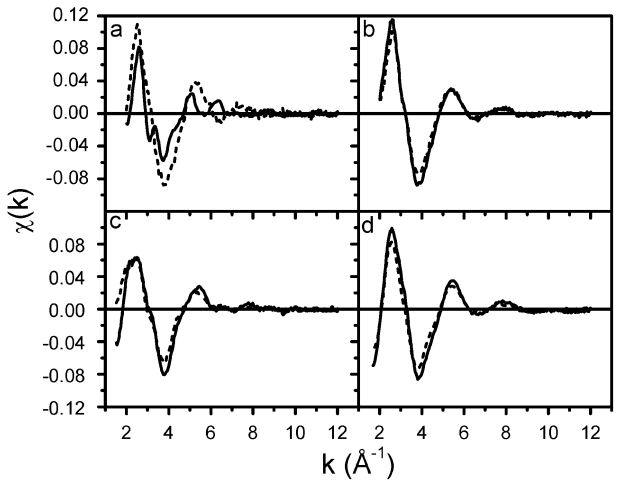

Fig. 2 Experimental EXAFS data ($\chi(k)$) after dehydration (- - -) and hydration (—) of (a) 1V–Si, (b) 1V–Nb, (c) 1V–Zr and (d) 1V–Al, all samples were measured at 77 K.

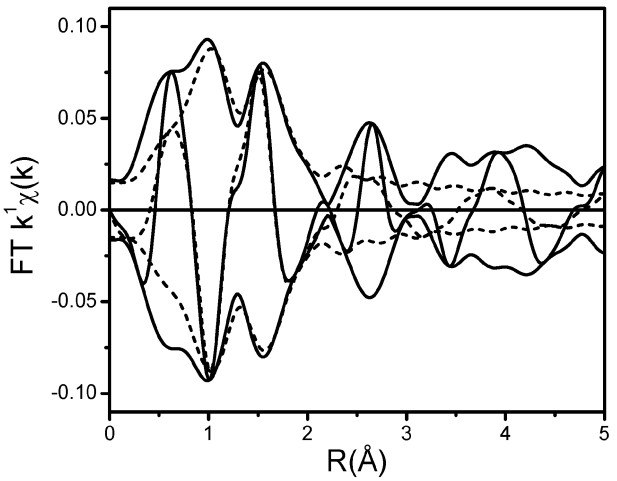

Fig. 4 The k^1 weighted FTs (Δk = 2.5–11 Å^{-1}) of the experimental $\chi(k)$ (—) for 1V–Si and the calculated three shell fit (- - -) in R-space (ΔR = 0.7–2.3 Å).

Table 2 EXAFS parameters obtained from R-space fits for 1V–Si–D (k^1, Δk = 2.5–11 Å^{-1}; ΔR = 0.7–4.0 Å) and for 1V–Si–H (three shell fit: k^1, Δk = 2.5–11 Å^{-1}; ΔR = 0.7–2.3 Å and total fit: k^1, Δk = 2.5–11 Å^{-1}; ΔR = 0.7–4.4 Å)

						Variances	
Sample	Scattering pair	N^a	R^a/Å	$\Delta\sigma^{2\,a}$	$\Delta E_0{}^a$	Imaginary part	Absolute part
1V–Si–D	V=O$_{(1)}$	1[b]	1.58[b]	−0.003	10.8	1.5	1.3
	V–O$_{(2)}$	3[b]	1.77	−0.002	0.1		
	V···Si$_{(3)}$	1[b]	2.61	0.015	5.0		
	V···O$_{(4)}$	2[b]	2.70	0.012	9.9		
	V···Si$_{(5)}$	1[b]	2.95	0.017	−4.4		
	V···O$_{(6)}$	1[b]	3.28	0.013	7.2		
	V···O$_{(7)}$	4[b]	3.69	0.014	−5.1		
1V–Si–H 3 shell fit	V=O$_{(1)}$	1[b]	1.58[b]	−0.004	7.7	3.5	2.4
	V–O$_{(2)}$	3	1.83	0.012	4.9		
	V···O$_{(3)}$	1	2.37	−0.001	7.2		
1V–Si–H total fit	V=O$_{(1)}$	1[b]	1.58[b]	−0.004	7.7	2.5	1.9
	V–O$_{(2)}$	3[b]	1.83[b]	0.012	4.9		
	V···O$_{(3)}$	1[b]	2.37[b]	−0.001	12.4		
	V···O$_{(4)}$	2	2.92	0.009	−14.4		
	V···Si$_{(5)}$	1	2.93	0.000	−10.4		
	V···V$_{(6)}$	1.4	3.18	0.017	−5.7		
	V···O$_{(7)}$	4	3.82	0.014	−13.3		

[a] N = coordination number (±10%), R = distance in Å (± 1%, $\Delta\sigma^2$ = Debye–Waller factor (±5%) and ΔE_0 = internal reference energy (±10%). [b] These parameters were fixed during the fitting procedure.

material and the coordination of other vanadium atoms in the vicinity of the absorber atom. The total R-space fit (k^1, Δk = 2.5–11 Å^{-1}, ΔR = 0.7–4.4 Å) has been applied with seven coordination shells. Since the number of allowed fit parameters is not infinite, we kept the coordination numbers and inter-atomic distances obtained from the three-shell fit constant. A structural model from Cerius[2] was used interactively during the fit process to verify coordinating atoms obtained from our fit. The final fit obtained in this way is presented in Fig. 5a and the fit parameters are listed in Table 2. It can be seen that the variances of the R-space fit are acceptable and lower than 3%.

A V···V coordination at 3.18 Å with average coordination number N = 1.4 has to be included in the fit. This V···V coordination was introduced to account for the new peak visible in the non-phase corrected FT around 2.8 Å, which was not observed in the 1V–Si–D sample.[29] A V···Si coordination was detected at 2.9 Å, almost 0.3 Å longer as detected in the 1V–Si–D sample.[29] Several V···O$_{support}$ coordination modes have to be included in the fit as well. The reliability of the fit of the higher coordination shells can be easily demonstrated by comparing the FT of the difference file (Raw − V–O$_{(1)}$ − V–O$_{(2)}$ − V–O$_{(3)}$) with the calculated higher shell contributions (V···O$_{(4)}$ + V···Si$_{(5)}$ + V···V$_{(6)}$ + V···O$_{(7)}$) (see Fig. 6a).

The analysis of the EXAFS data of 1V–Nb–H, 1V–Zr–H and 1V–Al–H showed that the small increase in intensity of the FTs between 0.5 < R < 1.5 Å after hydration is not due to a change in coordination geometry but due to a slight decrease in disorder of the first coordination sphere (V–O$_{(1)}$ and V–O$_{(2)}$). No observable changes are observed in the coordination geometry of the interface between the VO_4 cluster and the support. Small decreases in the Debye–Waller factors ($\Delta\sigma^2$) were needed to optimise the fit. However, for all three samples the EXAFS data analysis showed that a V···V coordination had to be included in the fit. The total R-space fits are displayed in Fig. 5b–d and the resulting coordination parameters are given in Tables 3–5.

The reliability of the fit of the higher coordination shells is demonstrated in Fig. 6b–d, which show the FT of the difference file (Raw − V–O$_{(1)}$ − V–O$_{(2)}$) with the calculated higher shell contributions (from support and nearby V). The EXAFS data analysis shows that the clustering of vanadium after hydration (as indicated by the V···V coordination number) is the largest for 1V–Si–H and decreases in the order 1V–Si > 1V–Nb > 1V–Zr > 1V–Al. The observed changes in the FT (2.5 < R < 3 Å after hydration seem to be smallest for 1V–Nb, while the fitted V···V contribution falls between 1V–Si and 1V–Zr. However, the FT of the V···V EXAFS in 1V–Nb–H and the fitted higher shell contributions, plotted in Fig. 7b, show that strong interference effects occur between the

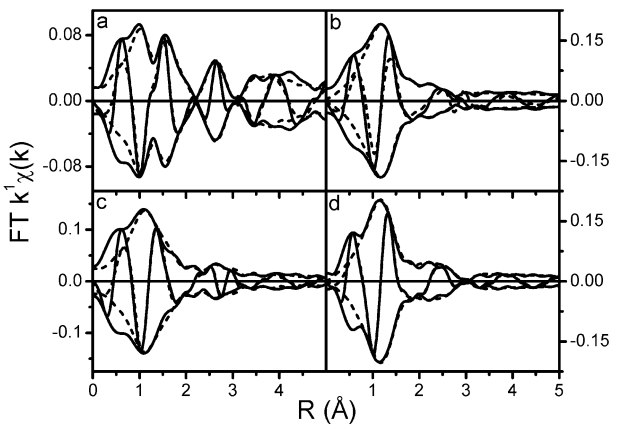

Fig. 5 The k^1 weighted FTs (Δk = 2.5–11 Å^{-1}, ΔR = 0.7–4.0 Å) of the experimental $\chi(k)$ (—) and the final fit (- - -) for (a) 1V–Si–H (b) 1V–Nb–H and (c) 1V–Zr–H and (d) 1V–Al–H.

Table 3 EXAFS parameters obtained from R-space fits for 1V–Nb–D (k^1, Δk = 2.5–11 Å^{-1}; ΔR = 0.7–3.5 Å) and for 1V–Nb–H (k^1, Δk = 2.5–11 Å^{-1}; ΔR = 0.7–4.4 Å)

						Variances	
Sample	Scattering pair	N^a	R^a/Å	$\Delta\sigma^{2\,a}$	$\Delta E_0{}^a$	Imaginary part	Absolute part
1V–Nb–D	$V{=}O_{(1)}$	1	1.58	0.001	10.4	0.8	0.7
	$V{-}O_{(2)}$	3	1.72	0.003	3.8		
	$V\cdots O_{(3)}$	1	2.43	0.004	−10.7		
	$V\cdots O_{(4)}$	1	2.64	0.006	0.9		
	$V\cdots Nb_{(5)}$	1	2.79	0.015	−6.1		
1V–Nb–H	$V{=}O_{(1)}$	1	1.58[b]	−0.003	10.4		
	$V{-}O_{(2)}$	3	1.72	0.001	3.8		
	$V\cdots O_{(3)}$	1	2.43	0.000	−10.7		
	$V\cdots O_{(4)}$	1	2.64	0.003	4.1	1.5	0.6
	$V\cdots Nb_{(5)}$	1	2.79	0.006	−5.5		
	$V\cdots V_{(6)}$	1.2	3.11	0.0234	14.0		

[a] N = coordination number (± 10%), R = distance in Å (± 1%), $\Delta\sigma^2$ = Debye–Waller factor (± 5%) and ΔE_0 = internal reference energy (10%). [b] This parameter was fixed during the fitting procedure.

EXAFS oscillations of the V···V and interface contributions. This explains why the observed changes in the FT induced by hydration seems to be small, while the analysis shows that the 1V–Nb sample has a considerable V···V contribution.

The EXAFS data analysis and the vanadium oxide cluster geometry for the dehydrated samples have been given and discussed extensively in previous studies.[28–29,38] The coordination parameters for the dehydrated samples are given in Tables 2–5 for 1V–Si, 1V–Nb, 1V–Zr and 1V–Al, respectively. After dehydration no V···V interactions were observed for the low loaded (1 wt%) samples, implying the presence of single isolated VO_4 clusters.

Discussion

1. XANES spectra

The XANES spectra of the dehydrated and hydrated supported vanadium oxide catalyst materials only showed clear differences for the 1V–Si sample. The decrease in pre-edge intensity indicated a change in the number of coordinating oxygen atoms around the central vanadium atom. For the other catalyst samples (1V–Al, 1V–Nb and 1V–Zr) only small differences in the XANES were observed, suggesting that the local configuration of the vanadium oxide cluster remains the same upon hydration. Yoshida *et al.* suggested that the fewer number of features in the first derivative of the XANES of a hydrated alumina supported catalyst results from the adsorption of water molecules on oxygen atoms in the vanadium oxide clusters, without changing the coordination symmetry.[39] For our samples only very minor changes were observed. These small changes in the XANES of 1V–Nb, 1V–Zr and 1V–Al upon hydration of the samples can be explained by the fact that our EXAFS analysis shows that the disorder decreases, while the overall structure remains the same. For the 1V–Si catalyst, profound changes were observed in the XANES. Our EXAFS analysis supported a considerable alteration in the vanadium oxide coordination.

Table 4 EXAFS parameters obtained from R-space fits for 1V–Zr–D(k^1, Δk = 2.5 –11 Å^{-1}; ΔR = 0.7–4.0 Å) and for 1V–Zr–H (k^1, Δk = 2.5–11 Å^{-1}; ΔR = 0.7–4.0 Å)

						Variances	
Sample	Scattering pair	N^a	R^a/Å	$\Delta\sigma^{2\,a}$	$\Delta E_0{}^a$	Imaginary part	Absolute part
1V–Zr–D	$V{=}O_{(1)}$	1	1.58	-0.002	10.0	1.3	1.0
	$V{-}O_{(2)}$	3	1.77	0.009	6.1		
	$V\cdots O_{(3)}$	1	2.38	0.012	−0.5		
	$V\cdots O_{(4)}$	1	2.64	0.011	8.0		
	$V\cdots Zr_{(5)}$	1	3.15	0.007	11.5		
	$V\cdots O_{(6)}$	1	3.25	0.009	0.6		
	$V\cdots O_{(7)}$	3	3.62	0.018	−6.4		
1V–Zr–H	$V{=}O_{(1)}$	1	1.58[b]	−0.003	15.9	1.8	1.4
	$V{-}O_{(2)}$	3	1.77	0.001	1.7		
	$V\cdots O_{(3)}$	1	2.38	0.000	−8.3		
	$V\cdots O_{(4)}$	1	2.64	0.006	−8.7		
	$V\cdots Zr_{(5)}$	1	3.15	0.004	12.0		
	$V\cdots V_{(6)}$	0.7	2.99	0.012	−11.0		
	$V\cdots O_{(7)}$	1	3.25	0.007	6.1		

[a] N = coordination number (±10%), R = distance in Å (±1%), $\Delta\sigma^2$ = Debye–Waller factor (±5%) and ΔE_0 = internal reference energy (10%). [b] This parameter was fixed during the fitting procedure.

Table 5 EXAFS parameters obtained from R-space fits for 1V–Al–D(k^1, Δk = 2.5–11 Å^{-1}; ΔR = 0.7–4.0 Å) and for 1V–Al–H (k^1, Δk = 2.5–11 Å^{-1}; ΔR = 0.7-4.0 Å)

						Variances	
Sample	Scattering pair	N^a	R^a/Å	$\Delta\sigma^{2\ a}$	$\Delta E_0{}^a$	Imaginary part	Absolute part
1V–Al–D	V═$O_{(1)}$	1	1.58	0.000	13.6	0.8	0.7
	V–$O_{(2)}$	3	1.72	0.008	3.1		
	V···$O_{(3)}$	1	2.30	0.013	−4.4		
	V···$Al_{(4)}$	1	3.10	0.015	6.8		
	V···$O_{(5)}$	2	3.50	0.008	−3.1		
	V···$O_{(6)}$	2	4.32	0.012	3.1		
1V–Al–H	V═$O_{(1)}$	1^b	1.58^b	−0.003	9.8	0.5	0.4
	V–$O_{(2)}$	3^b	1.72	0.002	2.0		
	V···$O_{(3)}$	1^b	2.30	0.009	−4.5		
	V···$V_{(4)}$	0.4^b	2.93	0.014	−1.8		
	V···$Al_{(5)}$	1^b	3.15	0.012	−6.0		
	V···$O_{(6)}$	2^b	3.50	0.002	−2.1		

^{a} N = coordination number (±10%), R = distance in Å (±1%), $\Delta\sigma^2$ = Debye–Waller factor (±5%) and ΔE_0 = internal reference energy (10%). ^{b} These parameters were fixed during the fitting procedure.

2. EXAFS data analysis: the number of independent parameters

When the V═O distance and coordination are taken as independent input for the EXAFS fit, 10 parameters are required to fit the coordination shells (V═$O_{(1)}$, V–$O_{(2)}$ and V–$O_{(3)}$) for the three-shell fit of the 1V–Si–H catalyst. Since 10.6 independent parameters are permitted for this fit, according to the Nyquist theorem, the data are not over fitted.[37]

Clearly, higher shell contributions cannot be ignored, as illustrated in Fig. 4. In order to determine the interface with the support oxide for the hydrated sample and possible coordination of other vanadium atoms the higher shells were incorporated in a new fit. According to the Nyquist theorem 22 parameters are allowed in the seven shell 1V–Si–H EXAFS fit, using Δk = 8.5 Å^{-1} and ΔR = 3.7 Å.[37] We used the distances and coordination numbers from the three-shell fit as independent input parameters for the seven-shell fit. For the seven-shell fit of 1V–Si–H this means that 22 free parameters ((7 shells × 4 parameters per shell) − 6 fixed input parameters) are required for the total fit (Table 2). Furthermore, a structural model obtained from Cerius[2] was used to verify the coordination of support atoms. The V–$O_{(2)}$ and V···$Si_{(4)}$ distances were interactively used as constraints for the model during the fitting process.

For the 1V–Al, 1V–Nb and 1V–Zr samples the small differences in coordination geometry, as observed in the XANES and FT of the raw EXAFS data, suggested that the interface with the support would be highly similar to the vanadium–support interface for the dehydrated samples. Therefore, the coordination numbers of and distances to the support atoms were regarded as independent input parameters

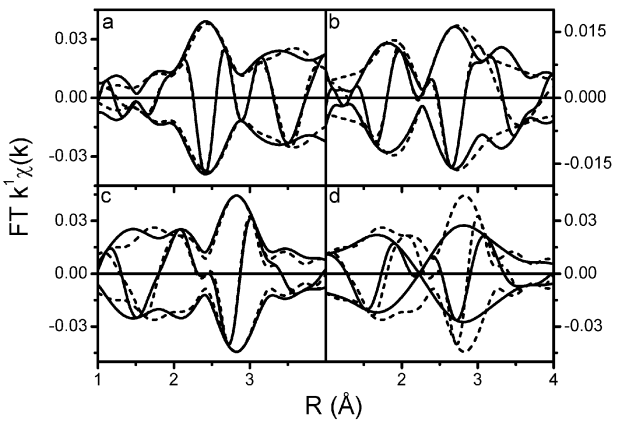

Fig. 6 The k^1 weighted FTs (Δk = 2.5–8 Å^{-1}) of the difference files for the direct oxygen coordination around vanadium (—) and the calculated higher shells from the support and vanadium (- - -). (a) ($Raw_{(1V-Si-H)} - O_{(1)} - O_{(2)} - O_{(3)}$) and $Si_{(4)} + V_{(5)} + O_{(6)} + O_{(7)}$; (b) ($Raw_{(1V-Nb\ -\ H)} - O_{(1)} - O_{(2)}$) and $O_{(3)} + O_{(4)} + Nb_{(5)} + V_{(6)}$; (c) ($Raw_{(1V-Zr-H)} - O_{(1)} - O_{(2)}$) and $O_{(3)} + O_{(4)} + Zr_{(5)} + O_{(6)} + V_{(7)}$; and (d) ($Raw_{(1V-Al-H)} - O_{(1)} - O_{(2)}$) and $O_{(3)} + Al_{(4)} + O_{(5)} + V_{(6)}$; the difference file shows that the higher shell contributions are nicely fit.

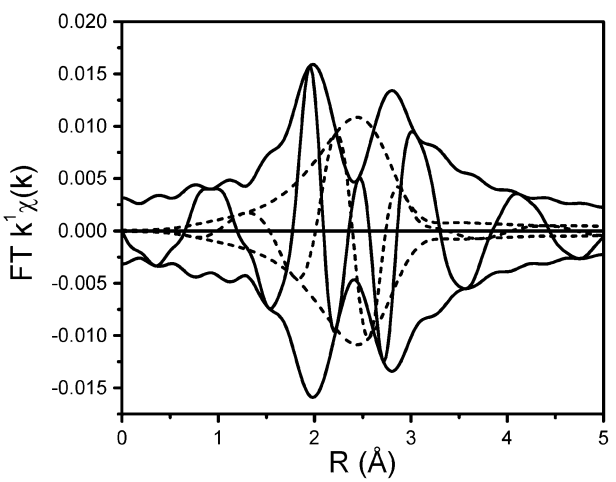

Fig. 7 The k^1 weighted FTs (Δk = 2.5–8 Å^{-1}) of the calculated contribution for $O_{(3)} + O_{(4)} + Nb_{(5)}$, (—) and the calculated higher shell from the vanadium atom ($V_{(6)}$), (- - -). The vanadium contribution is out of phase with the support atoms contribution ($O_{(3)} + O_{(4)} + Nb_{(5)}$), illustrating the reason for the small differences between the 1V–Nb–D and 1V–Nb–H FTs.

for these fits, together with the fourfold oxygen coordination in the first two shells and the V=O distance.

For the 1V–Al–H sample fit ranges of Δk = 2.5–11 Å^{-1} and ΔR = 0.7–4.0 Å were taken and six shells were incorporated in the fit. The number of allowed parameters was 19.8, while 16 were needed when the fourfold oxygen coordination and the support interface (coordination numbers and distances of three shells) obtained from the dehydrated model were regarded as independent input for the fit. The 1V–Zr has a fit range of Δk = 2.5–11 Å^{-1} and ΔR = 0.7–4 Å and a maximum of seven shells in the total fit. This means that 19.8 free parameters are available, while only 18 are needed when the fourfold coordination and the support interface are taken as fixed parameters. For the six-shell fit of the 1V–Nb catalyst 16 free parameters were needed, whereas 17.15 are available according to the Nyquist theorem (Δk = 2.5–11 Å^{-1}, ΔR = 0.7–3.5 Å). Summarizing, for all fits described in this paper the number of free parameters used stayed within the permitted value.

3. Structural consequences upon hydration: Influence of the net pH at the support surface on the molecular structure of vanadium oxide species

The differences between the 1V–Si–D and 1V–Si–H samples are already clearly visible from the XANES and the FT of the raw data as presented in Fig. 1 and 2, suggesting a significant change in the coordination geometry of the vanadium upon hydration of the sample. This was further supported by the EXAFS fit for the hydrated sample, from which we may conclude that the oxygen coordination around vanadium changed from four to five atoms, the V···Si distance enlarged and a V···V contribution had to be included in the fit. The lengthening of the V···Si distance from 2.65 to 2.93 Å involves changes in the distances to the other support atoms as well. From the Cerius[2] model, depicted in Fig. 8, it was concluded that an O atom from the Si–O–Si bridge could be observed at 2.92 Å. Moreover, the clustering of the vanadium oxide species resulted in the observation of another O atom at 2.92 Å from the neighbouring vanadium oxide cluster. In other words, the combination of the structural model with the EXAFS analysis yielded a tool enabling the fit of higher coordination shells.

Smaller differences were observed in both XANES and the FT of the raw data for the vanadium oxide species supported on the other three support oxides. The increase in intensity in the $0.7 < R < 1.7$ Å region upon hydration is not the outcome of an alteration in the first coordination shell, but results from the decrease in the Debye–Waller factor, *i.e.* better arrangement of the oxygen atoms around the vanadium atom. Although the coordination symmetry of the oxygen atoms around the central vanadium did not seem to change, as already observed for alumina-supported vanadium oxide by Yoshida *et al.*, differences in the FT above R = 2 Å could be observed for the 1V–Al and 1V–Zr samples.[39] These differences indicate a change in the higher shell coordination, which was incorporated in the fit by adding a V contribution. The structure of the interface with the support material remained the same for the alumina-, niobia- and zirconia-supported vanadium oxide catalysts, indicating that a major surface reconstruction upon hydration was not required to explain the differences between the spectra for the hydrated and dehydrated catalyst samples. In addition, the disorder in the interface contribution decreases, resulting in lower Debye–Waller factors. For the 1V–Nb sample, the higher shell part of the FT hardly seemed to change upon hydration of the sample, only very small variations in the imaginary part around 2.5–3 Å were observable. However, a vanadium contribution must be included to fit the data in a satisfactory manner. As illustrated in Fig. 7 the calculated vanadium contribution is in anti-phase with the other contributions in the higher shells. This anti-phase effect leads to the cancellation of this contribution in the total spectrum, explaining the minor variations between the dehydrated and hydrated spectrum for the 1V–Nb sample.

So, all hydrated spectra required the inclusion of a vanadium contribution to complete the fit, indicating that the vanadium oxide species (at least partially) cluster upon hydration. The clustering of vanadium oxide species has been suggested previously in literature by several authors on the basis of Raman measurements.[4,8,18,19] The formation of the aggregates seems to be reversible, since the Raman and UV-VIS spectra of reoxidated samples are exactly the same as those of the dry samples. In addition the OH-stretch region in the IR spectra showed the formation of V–OH bonds upon hydration, while the corresponding 3660 cm^{-1} band disappeared during reoxidation at elevated temperatures.[38] Furthermore the color change (white to yellow/orange) observed for the silica supported sample upon hydration is reversible as well. The type of molecular species present in the hydrated samples is usually determined through comparison of the spectral features with reference compounds.[5,19] With EXAFS, Silversmit *et al.* detect additional cations in their hydrated sample (CN = 2, R = 3.5 Å), however, they did not distinguish between the support cation (Ti) and a neighbouring vanadium atom.[14] Inumaru *et al.* concluded on the basis of the FT of their EXAFS data that the V···V contribution in their spectrum increased with the support material: MgO < Al_2O_3 < SiO_2.[20]

The molecular structure of vanadium oxide species on a fully hydrated catalyst is dictated by the concentration of the vanadium oxide species and the pH of the water layer on top of the support surface, which in turn is determined by the PZC of the support oxide.[4] Since the vanadium oxide loading is low

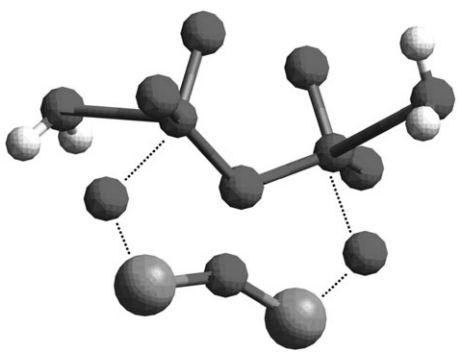

Fig. 8 Graphical representation of the hydrated vanadium oxide cluster on a silica support.

Table 6 Predicted vanadium oxide structures for hydrated catalyst samples with the average V···V coordination number as a function of the support oxide material, together with the observed average V···V coordination number by a detailed EXAFS analysis

Support material	Predicted structures[4]	Predicted range of average V···V coordination number	Observed average V···V coordination number
SiO_2	V_2O_5, $V_{10}O_{26}(OH)_2$, $VO(OH)_3$	0–≤ 4	1.4
Nb_2O_5	$V_{10}O_{27}(OH)$ $(VO_3)_n$	1.8; 0–≤ 2	1.2
ZrO_2	$VO_2(OH)_2$, $(VO_3)_n$	0–≤ 2	0.7
Al_2O_3	$VO_3(OH)$, V_2O_7	0–1	0.4

for the catalysts under investigation, changes observed in the molecular structure are mainly determined by the properties of the support oxide materials. Based on the predominance diagram and the PZC of the support surface Wachs and co-workers proposed that upon hydration low-loaded silica-supported vanadium oxide catalysts contained a mixture of V_2O_5, $V_{10}O_{26}(OH)_2$ and $VO(OH)_3$, whereas for low-loaded alumina-supported vanadium oxide catalysts $VO_3(OH)$ and V_2O_7 were predicted to be present (Table 6).[4,5,22,23]

Although the exact value of the PZC may vary with the support oxide type,[4,40–43] the trend in PZC for the different support materials is in line with the sequence reported by Deo *et al.*: MgO > γ-Al_2O_3 > TiO_2 > ZrO_2 > Nb_2O_5 > SiO_2.[4] The same trend in PZC values was experimentally observed for the support oxides presented in this paper (Table 1). The exact molecular structure of the hydrated vanadium oxide species and the extent of vanadium oxide clustering are indeed a function of the support oxide material, as is summarized in Table 7. In Fig. 9 the relation between the type of support oxide and the vanadium oxide clustering is shown. The V···V coordination number increases when the support pH at PZC value decreases. These results are in line with the prediction made by the group of Wachs, which suggested larger clusters as the pH at PZC decreased.[4,5,22,23] A similar result was observed by Inumaru *et al.* who showed that the V···V contribution in their FT of the EXAFS data of vanadium oxide supported on SiO_2, Al_2O_3 and MgO decreased when the support material changed from SiO_2 to MgO, although they did not include a V···V contribution in their fit and did not obtain V···V coordination numbers.[20] In addition to the formation of larger clusters we have found a relation between the support pH at PZC and the V···V distance, as is shown in Fig. 9. The V···V distance decreased, while the pH at PZC of the support increased (increasing cluster size).

Table 6 compares the structures for low-loaded hydrated supported vanadium oxide catalysts predicted by Wachs and co-workers to the coordination numbers obtained from our EXAFS fits.[4] For 1V–Al and 1V–Zr the observed V···V coordination number lies within the predicted range, suggesting that a mixture of the two predicted vanadium oxide structures is formed. In the case of 1V–Al the observed coordination number can be explained by the presence of a mixture of 60% $VO_3(OH)$ and 40% V_2O_7. Both molecular structures have an oxygen coordination of 4, which is in agreement with the EXAFS results (Tables 5 and 8). The 1V–Zr sample has an observed V···V coordination number of 0.7 and the vanadium species has a fourfold oxygen coordination. Although both predicted structures are supported by the EXAFS oxygen coordination numbers, the V···V coordination again indicates the presence of a mixture of structures. When $(VO_3)_n$ has an infinite chain length ($CN_{V\cdots V}$ = 2), 35% of the vanadium atoms will be found in $(VO_3)_n$ chains and 65% in monomeric $VO_2(OH)_2$. However, it is very possible that the $(VO_3)_n$ chain lengths do not reach infinity, resulting in a lower average V···V coordination number per chain. Consequently, a larger percentage of the vanadium atoms will be incorporated in chains in order to reach the observed average V···V coordination number of 0.7. For 1V–Nb $V_{10}O_{27}(OH)$ and $(VO_3)_n$ are the predicted structures. However, our EXAFS and XANES indicated that the majority of the species has a fourfold coordination, suggesting only minimal amounts of $V_{10}O_{27}(OH)$ may be formed. The V···V coordination number of 1.2 indicates either short $(VO_3)_n$ chain lengths (n = 2, 3) or a combination of monomeric and polymeric species. If $(VO_3)_n$ has an infinite chain length ($CN_{V\cdots V}$ = 2), 60% of the vanadium atoms will be found in $(VO_3)_n$ chains, while 40% of the vanadium atoms must be present in a monomeric configuration. The results from 1V–Si clearly indicated the presence of vanadium oxide species with an oxygen coordination higher than four, which is in agreement with the prediction of $V_{10}O_{26}(OH)$ and V_2O_5 to be present. The combination of these two molecular structures would lead to a high V···V coordination number (Table 8), however a value of only 1.4 has been observed. This lower value again suggests the presence of a mixture of both polymeric and monomeric species. Indeed the presence of $VO(OH)_3$ was also predicted (Table 6).

Not only the V···V coordination and distances were determined in this EXAFS study, the V···M^+ distance to the support cation was also estimated for the hydrated and dehydrated samples (Table 7). The V···M^+ distance depends

Table 7 EXAFS coordination parameters and inter-atomic distances for all catalysts under dehydrated and hydrated conditions to facilitate an easy comparison between different catalysts as a function of support oxidation material and the hydration degree

	1V–Si		1V–Nb		1V–Zr		1V–Al	
	D[a]	H[a]	D[a]	H[a]	D[a]	H[a]	D[a]	H[a]
$CN_{V\cdots V}$	0	1.4	0	1.2	0	0.7	0	0.4
$R_{V\cdots V}$ (Å)	—	3.18	—	3.11	—	2.99	—	2.93
$R_{V\cdots M}$ (Å)	2.61	2.93	2.79	2.79	3.20	3.15	3.10	3.15

[a] D = dehydrated, H = hydrated.

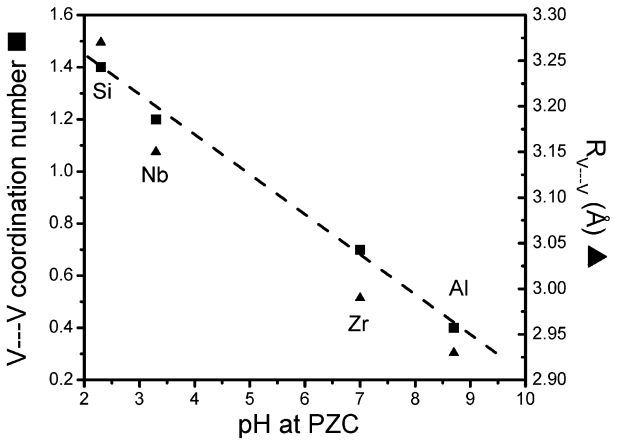

Fig. 9 The V···V coordination number (■) and distance (▲) as a function of the support cation. Both V···V coordination number and distance increase when the support oxide pH at PZC value decreases.

a little on the support oxide and in case of silica changes with the degree of hydration. From clay-like substances, as well as on goethite, $V\cdots M^+$ distances of ~3 Å were determined for adsorbed vanadium species, which is in the range of the distances observed for our catalyst samples.[44–46] Wehrli *et al.* have shown on alumina and titania that the adsorption of vanadium oxide species is fairly strong and probably takes place *via* an inner-sphere type mechanism.[47,48] Extrapolating this idea to the other support oxides, the $V\cdots M^+$ distances suggest an adsorption mechanism similar to the one on alumina for niobia and zirconia as well. However, on silica the adsorption may take place *via* another mechanism, resulting in an enlarged $V\cdots M^+$ distance for the hydrated species with respect to the dehydrated species.

Concluding, the combination of the structural model with the EXAFS analysis resulted in the determination of not only the direct oxygen coordination around hydrated vanadium oxide species, but also enabled the fit of higher shell contributions to the spectrum. The V···V coordination numbers obtained from the higher shells clearly showed that the degree of vanadium oxide clustering depends on the type of oxide support.

Conclusions

The effect of the support oxide, *i.e.*, Al_2O_3, Nb_2O_5, SiO_2 and ZrO_2, on the molecular structure of hydrated vanadium oxide species has been investigated with EXAFS spectroscopy for low-loaded supported vanadium oxide catalysts. The silica-supported vanadium oxide catalyst exhibited a clear alteration in the coordination environment around the central vanadium atom upon hydration and the oxygen coordination around vanadium increased to five. Only minor changes in the oxygen coordination were detected for the alumina-, niobia- and zirconia-supported vanadium oxide catalysts; *i.e.*, the fourfold oxygen coordination was maintained. Moreover, the structure of the interface with the support material remained almost the same for the alumina-, niobia- and zirconia-supported vanadium oxide catalysts as well, suggesting a strong adsorption interaction of the vanadium oxide species with the support surface.

The vanadium oxide species were found to form larger clusters upon hydration. The number of vanadium atoms in the second coordination shell increased with decreasing PZC of the support oxide; *i.e.*, $Al_2O_3 < ZrO_2 < Nb_2O_5 < SiO_2$. The combination of the structural model with the EXAFS analysis resulted in the determination of the direct oxygen coordination in hydrated vanadium oxide species and the fit of higher shell contributions to the spectrum. The V···V coordination numbers obtained from the higher shells clearly showed that the degree of clustering depends on the type of support material. On all support oxides different mixtures of monomeric and polymeric hydrated vanadium oxide structures were found to be present and the semi-quantitative distribution of vanadium oxide species obtained is in general agreement with earlier developed predictions based on Raman spectroscopy.

Table 8 Common vanadium oxide structures with their oxygen coordination and the average V···V coordination number

Type of structure	Oxygen coordination around V	Average V···V coordination number[a]
VO_4	4	0
V_2O_7	4	1
V_3O_9	4	1.33
V_4O_{12}	4	1.5
$(VO_3)_n$	4	≤2
$V_{10}O_{28}$	6	1.8
V_2O_5	6	≤4

[a] Coordination number based on the nearest vanadium neighbour.

References

1 T. Machej, J. Haber, A. M. Turek and I. E. Wachs, *Appl. Catal.*, 1991, **70**, 115–128.
2 P. Van Der Voort, M. G. White, M. B. Mitchell, A. A. Verberckmoes and E. F. Vansant, *Spectrochim. Acta, Part A*, 1997, **53**, 2181–2187.
3 G. T. Went, S. T. Oyama and A. T. Bell, *J. Phys. Chem.*, 1990, **94**, 4240–4246.
4 G. Deo, I. E. Wachs and J. Haber, *Crit. Rev. Surf. Chem.*, 1994, **4**, 141–187.
5 G. Deo and I. E. Wachs, *J. Phys. Chem.*, 1991, **95**, 5889–5895.
6 X. Gao and I. E. Wachs, *J. Phys. Chem. B*, 2000, **104**, 1261–1268.
7 J.-M. Jehng, G. Deo, B. M. Weckhuysen and I. E. Wachs, *J. Mol. Catal. A: Chem.*, 1996, **110**, 41–54.
8 M. F. Hazenkamp and G. Blasse, *J. Phys. Chem.*, 1992, **96**, 3442–3446.
9 S. Yoshida, T. Tanaka, T. Hanada, T. Hiraiwa, H. Kanai and T. Funabiki, *Catal. Lett.*, 1992, **12**, 277–286.
10 B. Solsona, T. Blasco, J. M. López Nieto, M. L. Peña, F. Rey and A. Vidal-Moya, *J. Catal.*, 2001, **203**, 443–452.
11 M. Anpo, M. Sunamoto and M. Che, *J. Phys. Chem.*, 1989, **93**, 1187–1189.
12 M. Morey, A. Davidson, H. Eckert and G. Stucky, *Chem. Mater.*, 1996, **8**, 486.
13 U. G. Nielsen, N.-Y. Topsoe, M. Brorson, J. Skibsted and H. J. Jakobsen, *J. Am. Chem. Soc.*, 2004, **126**, 4926–4933.
14 G. Silversmit, J. A. van Bokhoven, H. Poelman, A. M. J. van der Eerden, G. B. Marin, M.-F. Reyniers and R. De Gryse, *Appl. Catal., A*, 2005, **285**, 151–162.
15 M. Ruitenbeek, A. J. van Dillen, F. M. F. de Groot, I. E. Wachs, J. W. Geus and D. C. Koningsberger, *Top. Catal.*, 2000, **10**, 241–254.
16 M. Ruitenbeek, Ph.D. thesis, Universiteit Utrecht, Utrecht, The Netherlands, 1999, p. 22.
17 M. Ruitenbeek, F. M. F. de Groot, A. J. van Dillen and D. C. Koningsberger, *Stud. Surf. Sci. Catal.*, 2000, **130D**, 3101–3106.

18 X. Gao, S. R. Bare, B. M. Weckhuysen and I. E. Wachs, *J. Phys. Chem. B*, 1998, **102**, 10842–10852.
19 M. A. Vuurman and I. E. Wachs, *J. Mol. Catal.*, 1992, **77**, 29–39.
20 K. Inumaru, M. Misono and T. Okuhara, *Appl. Catal., A*, 1997, **149**, 133–149.
21 C. F. Baes, Jr and R. E. Mesmer, *The Hydrolysis of Cations*, John Wiley and Sons, New York, 1976, p. 210.
22 M. A. Bañares and I. E. Wachs, *J. Raman Spectrosc.*, 2002, **33**, 359–380.
23 B. M. Weckhuysen and I. E. Wachs, in *Handbook of Surfaces and Interfaces of Materials*, ed. H. S. Nalwa, Academic Press, San Diego, 2001, vol. 1, p. 613.
24 B. M. Weckhuysen, L. M. de Ridder and R. A. Schoonheydt, *J. Phys. Chem.*, 1993, **97**, 4756–4763.
25 F. W.H. Kampers, T. M. J. Maas, J. van Grondelle, P. Brinkgreve and D. C. Koningsberger, *Rev. Sci. Instrum.*, 1989, **60**, 2635–2638.
26 M. Vaarkamp, J. C. Linders and D. C. Koningsberger, *Physica B (Amsterdam)*, 1995, **208/209**, 159.
27 D. C. Koningsberger, B. L. Mojet, G. E. van Dorssen and D. E. Ramaker, *Top. Catal.*, 2000, **10**, 143–155.
28 D. E. Keller, F. M. F. de Groot, D. C. Koningsberger and B. M. Weckhuysen, *J. Phys. Chem. B*, 2005, **109**, 10223–10233.
29 D. E. Keller, D. C. Koningsberger and B. M. Weckhuysen, *J. Phys. Chem. B*, 2006, **110**, 14313–14325.
30 G. G. Li, F. Bridges and C. H. Booth, *Phys. Rev. B: Condens. Matter*, 1995, **52**, 6332.
31 *Cerius,*^{2}, Molecular Simulations Inc., San Diego, CA, 1997.
32 M. L. Ferreira and M. Volpe, *J. Mol. Catal. A: Chem.*, 2002, **184**, 349–360.
33 R.-S. Zhou and R. L. Snyder, *Acta Crystallogr., Sect. B: Struct. Sci.*, 1991, **47**, 617–630.
34 A. W. Stobbe-Kreemers, G. C. van Leerdam, J.-P. Jacobs, H. H. Brongersma and J. J. F. Scholten, *J. Catal.*, 1995, **152**, 130–136.
35 R. Gruehn, *J. Less-Common Met.*, 1966, **11**, 119–126.
36 J. Wong, F. W. Lytle, R. P. Messmer and D. H. Maylotte, *Phys. Rev. B: Condens. Matter*, 1984, **30**, 5596–5610.
37 E. A. Stern, *Phys. Rev. B: Condens. Matter*, 1993, **48**, 9825–9827.
38 D. E. Keller, T. Visser, F. Soulimani, D. C. Koningsberger and B. M. Weckhuysen, *Vib. Spectrosc.*, 2006, DOI: 10.1016/j.vibspec.2006.07.005.
39 S. Yoshida, T. Tanaka, Y. Nishimura, H. Mizutani and T. Funabiki, in *Proceedings of the 9th International Congress on Catalysis*, ed. M. J. Philips and M. Ternan, Chemical Institute of Canada, Calgary, 1988, **3**, pp. 1473–1480.
40 T. Blasco and J. M. López Nieto, *Appl. Catal., A*, 1997, **157**, 117.
41 M. Kosmulski, *J. Colloid Interface Sci.*, 2004, **275**, 214–224.
42 M. Kosmulski, *J. Colloid Interface Sci.*, 2002, **253**, 77–87.
43 M. Kosmulski, *Langmuir*, 1997, **13**, 6315–6320.
44 C. L. Peacock and D. M. Sherman, *Geochim. Cosmochim. Acta*, 2004, **68**, 1723–1733.
45 V. Rives, F. M. Labajos, M. A. Ulibarri and P. Malet, *Inorg. Chem.*, 1993, **32**, 5000–5001.
46 P. Malet, J. A. Odriozola, F. M. Labajos, V. Rives and M. A. Ulibarri, *Nucl. Instrum. Methods Phys. Res., Sect. B*, 1995, **97**, 16–19.
47 B. Wehrli and W. Stumm, *Geochim. Cosmochim. Acta*, 1989, **53**, 69–77.
48 B. Wehrli and W. Stumm, *Langmuir*, 1988, **4**, 753–758.
49 A. Khodakov, B. Olthof, A. T. Bell and E. Iglesia, *J. Catal.*, 1999, **181**, 205–216.

